IRAQI JOURNAL OF APPLIED PHYSICS
Vol. 22, No. 1, January-March 2026, pp. 7-11

Z-Scan Characterization of Hybrid Alq_3–Gold Nanostructures for Enhanced Nonlinear Optics

Noor Al-Huda H. Rashid *
Lamees A. Abdullah

Department of Physics,
College of Science,
University of Baghdad,
Baghdad, IRAQ
* Corresponding author:
noorhudahasan12567@gmail.com

In this study, the linear and nonlinear optical properties of gold nanoparticles (AuNPs) and their nanocomposites with tris(8-hydroxyquinoline)aluminum (Alq_3) were examined. The gold nanoparticles were synthesized using pulsed laser ablation in chloroform. XRD results confirmed that the nanoparticles had a face-centered cubic structure, with an average particle size around 7 nm. The UV–visible spectroscopy showed a clear peak at 340 nm, indicating the surface plasmon resonance of gold nanoparticles, with a blue shift observed upon the addition of Alq_3, indicating strong interaction within the nanocomposite. Alq_3:AuNPs nanocomposites were prepared in three volume ratios: 2:1, 2:2, and 1:2. Nonlinear optical measurements were performed using the Z-scan technique, which showed that the samples had negative nonlinear refractive indices around 10^{-11} m²/W, consistent with self-defocusing effects. Among the tested samples, pure Alq_3 showed the highest third-order nonlinear behavior. However, the Alq_3:AuNPs (2:1) nanocomposite exhibited a clear improvement when compared to the response of pure AuNPs, suggesting that adding Alq_3 enhances the nonlinear behavior of gold nanoparticles through a synergistic effect.

Keywords: Z-scan technique; Alq_3 complex; Gold nanoparticles; Nonlinear optics
Received: 4 May 2025; Revised: 26 June 2025; Accepted: 2 July 2025; Published: 1 January 2026

1. Introduction

The demand for nanoparticles has increased recently because of their applications in energy, catalysis, materials and medicine [1]. The size, surface morphology of nanoparticles, and shape are vital in determining their physical, optical, electrical, and chemical properties. Chemical reduction of metal ions, chemical vapor deposition (CVD), electrochemical synthesis and physical vapor deposition (PVD) are all methods used for preparing metal nanoparticles [2]. However, the chemicals used in these syntheses are usually hazardous, expensive, and harmful to the environment. Gold nanoparticles' exceptional physical and chemical characteristics have garnered a lot of interest, and they have been used in a variety of industries, including optics [3], catalysis [4], and biomedical applications [5].

The optical response of gold nanoparticles is strongly influenced by their size and shape, which can be tuned through different synthesis methods [6]. Among these, pulsed laser ablation is a clean and efficient physical technique that produces high purity nanoparticles in liquid media without the use of surfactants or reducing agents. Metals like gold and copper often display vivid colors due to surface plasmon resonance (SPR). This phenomenon occurs when conduction band electrons respond collectively to an external electromagnetic wave [7]. When gold nanoparticles are incorporated into polymers, this interaction can be further amplified. The result is not just a change in appearance, but an improvement in their optical functionality, including nonlinear effects like reverse saturable absorption and nonlinear refraction.

Tris(8-hydroxyquinoline)aluminum (Alq_3) is an organometallic compound that has been widely used in optoelectronic applications, especially in organic light-emitting diodes (OLEDs), due to its high thermal stability, efficient fluorescence, and good electron-transport capabilities [8-13]. However, its intrinsic nonlinear optical performance is relatively weak, which limits its use in advanced optical modulation systems [14].

Recent studies have shown that integrating metal nanoparticles with organic semiconductors can significantly improve their nonlinear optical responses [15-16]. However, studies focusing on the nonlinear optical properties of Alq_3 when combined with laser synthesized gold nanoparticles are still limited, and the influence of different mixing ratios on the optical response remains largely unexplored. In this study, gold nanoparticles were synthesized using pulsed laser ablation in chloroform and subsequently combined with Alq_3 at various volume ratios. Structural analysis was performed using X-ray diffraction (XRD). In addition, the optical properties of the colloidal samples were examined using UV–visible spectroscopy and the Z-scan technique.

2. Materials and Methods

Gold nanoparticles (AuNPs) were synthesized using the laser ablation technique. A gold target, 0.5 mm thick and 99.99% pure, was immersed in a beaker containing 10 ml of chloroform with similar purity. The

setup was exposed to vertical irradiation from a Q-switched Nd:YAG laser operating at 1064 nm with a pulse duration of approximately 7 ns, a beam spot size of about 0.5 mm² and a repetition rate of 3 Hz. The laser beam was concentrated onto the gold layer by means of a lens having a focal length of 20 cm. The laser energy was set to 500 mJ, and a total of 1500 pulses were used during the process. A simple diagram of the laser ablation setup is presented in Fig. (1). This technique was preferred over chemical reduction methods due to its capability to generate high-purity AuNPs free of surfactants or residual chemicals, providing better control over particle size and optical characteristics.

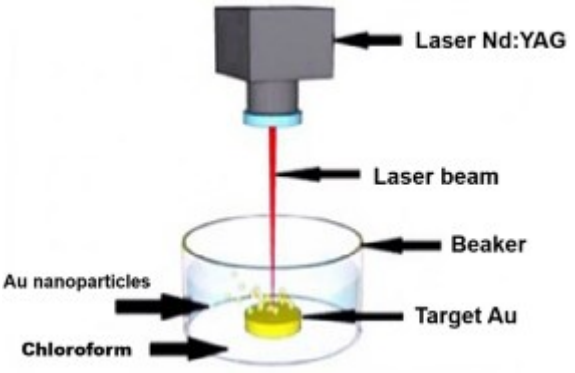

Fig. (1) Schematic diagram of the laser ablation method

For the preparation of the composite solution, 3 mg of Alq_3 was completely dissolved in 20 ml of chloroform (also 99.99% pure). Chloroform was chosen not only due to its excellent solubility of Alq_3 but also because it helps maintain AuNPs dispersion without negatively affecting their optical properties. The mixture was stirred magnetically at room temperature for an hour to ensure full dissolution. Afterward, this Alq_3 solution was blended with the gold nanoparticles in varying volume ratios: 2:1, 2:2, and 1:2. These mixtures were placed in test tubes and treated with ultrasound for one minute to improve the dispersion. Finally, the samples were deposited onto glass slides using the spin coating technique at 1500 rpm for 15 seconds. The coated slides were then placed in an oven at 60°C for one hour to allow the films to dry completely.

The structural properties of the AuNPs were analyzed using X-ray diffraction (XRD). The linear optical properties were studied using a UV-Visible spectrophotometer, while the nonlinear optical properties of the Au and Alq_3:AuNPs were measured using the Z-scan technique based on the method of Sheik-Bahae et al. [16]. The setup included a CW laser diode with a wavelength of 405 nm and a focusing lens with an 8.5 cm focal length. The beam diameter at the focal point was around 4 mm. The samples were placed in 10 mm thick quartz cells. A beam splitter, optical filters, and a detector were used to control and measure the laser beam. The detector was connected to a controller, which was linked to a computer for data collection. The controller allowed adjusting sensitivity and gain depending on the sample's transmittance. The sample was moved along the Z-axis around the focal point to measure the nonlinear response. Figure (2) shows the experimental setup for the Z-scan technique.

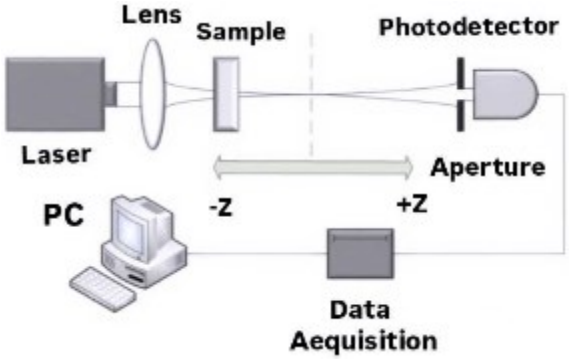

Fig. (2) Experimental setup of Z-Scan technique

The n_2 values are calculated using the following equations (1) and (2) [17]

$$n_2 = \frac{\Delta\varphi_o}{KI_oL_{eff}} \quad (1)$$

$$\Delta\varphi_0 = \frac{\Delta Lp-v}{0.406(1-T_a)0.25} \quad (2)$$

where $\Delta\varphi_0$ is the nonlinear phase shift at the focus, L_{eff} is the effective thickness of the sample. $K=2\pi/\lambda$ wavevector, I_0 equals to 2.02347 Mw/m^2 intensity of the laser beam at focus (z =0) , ΔL_{p-v} is the difference between the normalized peak and valley transmission. The nonlinear absorption coefficient β, was obtained from the open aperture z-scan technique by [17]

$$\beta(m/W) = \frac{2\sqrt{2}\Delta T}{L_{eff}I_0} \quad (3)$$

where ΔT is the one peak or one valley at the open aperture Z-scan curve. T_a is the aperture transmittance and is given by [17]

$$T_a = 1 - exp\left[-\frac{2r_a^2}{w_a^2}\right] \quad (4)$$

where r_a is 1mm aperture radius, w_a is 4mm beam radius at the aperture. L=10 mm thickness of the sample. F is focal length, A is the absorbance at 405 nm, α is the coefficient of the linear absorption α=2.303 A/L (22), where λ is the wavelength of the beam, L_{eff} is the effective length of the sample, and the following relationship can determine it [17]

$$L_{eff} = \frac{(1-exp(-\alpha L))}{\alpha} \quad (5)$$

3. Results and Discussion

Figure (3) shows the XRD pattern of Au nanoparticles. A cubic polycrystalline structure with the peak positions shown in Fig. (3) is observed to be consistent with the standard data obtained from JCPDS

card 04-0784. The Bragg's angle (2θ) was at 38.9°, 45°, 65°, and 78° and its reflection levels were (111), (200), (220), and (311), indicating that have a polycrystalline structure with face-centered cubic (F.C.C.) phase structure. The corresponding crystalline size of the prepared Au nanoparticles was calculated according to the Williamson-Hall analysis [18]. The average crystallite size was estimated to be 7 nm.

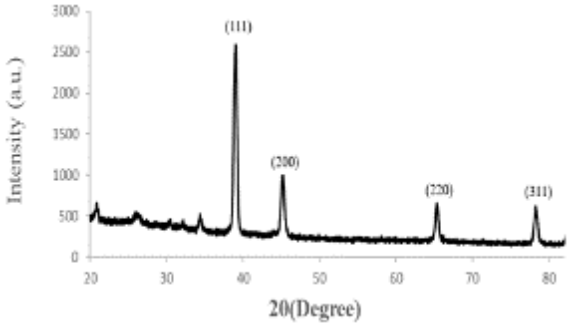

Fig. (3) XRD pattern of Au nanoparticles

The absorption behavior of Au nanoparticles was examined using a Metertech SP-8001 UV–Visible spectroscopy in the range of 300–600 nm. Figure (4) shows the absorption spectrum of Au nanoparticles. The relationship between absorbance and wavelength is an exponential decay, with the absorbance spectrum peak at 340 nm. This peak is noticeably blue-shifted compared to the typical surface plasmon resonance (SPR) range (520–550 nm) for Au nanoparticles. This shift may be attributed to the small particle size (~7 nm) and the dielectric nature of the chloroform solvent. Additionally, interband transitions or solvent-related effects might also contribute to this unusual absorption behavior. The absorption spectrum of pure Alq_3 and Alq_3:AuNPs in the wavelength range 300-700nm is shown in Fig. (5). The relationship between absorbance and wavelength is an exponential decay of absorbance spectrum of Alq_3 peaking at 416 nm. It is also observed from the absorption that when Au is mixed with the Alq_3, there is a shift in the absorption spectrum towards shorter wavelengths (blueshift). This occurs because the photons not absorbed by Alq_3 penetrate the Au, where they are absorbed. Therefore, we noticed an increase in the absorption width, with the best results appearing at the ratio of 2:2. This can be used as a detector for ultraviolet radiation.

Tauc's plot can be used to determine the energy band gap (E_g), where hv is the photon energy and the direct band gap is determined on the abscissa and $(\alpha hv)^2$ on the ordinate can be calculated from the equation [19]

$$(\alpha hv)^2 = c(hv - E_g) \quad (6)$$

where c is a constant, h is the Planck's constant, α is the absorption coefficient, v is the frequency

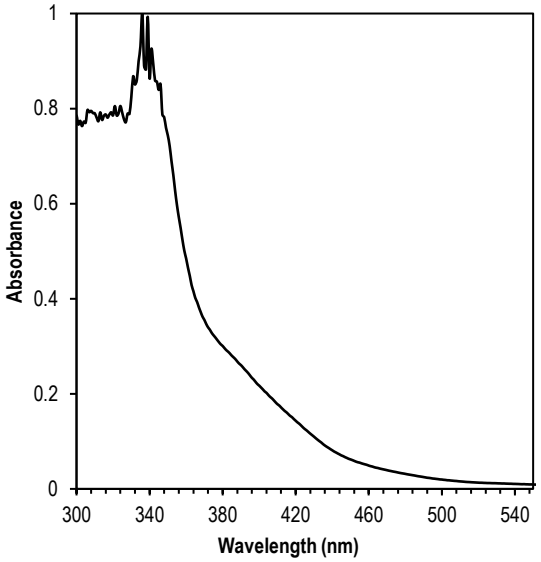

Fig. (4) Absorption spectrum of Au nanoparticles

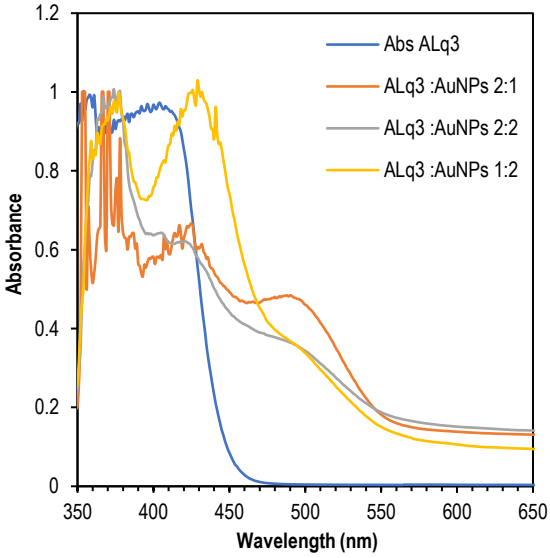

Fig. (5) Absorption spectra of pure Alq_3 and Alq_3:AuNPs with different concentrations

As shown in Fig. (6), the intersection of the straight line with the horizontal axis (photon energy (hv)) gives the optical energy band gap of about 2.94 eV. The Au nanoparticles exhibit local surface plasmon resonance (LSPR), where free electrons oscillate collectively under light excitation [20]. Nanogold does not possess a traditional energy gap but exhibits a spectral response similar to an energy gap due to surface plasmons. Therefore, the band gap obtained from the Tauc's plot should be interpreted as a pseudo-band gap, reflecting the onset of interband transitions or plasmonic absorption, rather than a true electronic band gap. This value helps quantify the optical activity range of the Au nanoparticles. Also in Fig. (7), where the intersection of the straight line with the horizontal axis (hv) gives

the optical energy band gap for pure Alq_3 and Alq_3:AuNPs with (1:2), (2:2), and (2:1) ratios, which are approximately 2.84, 3.47, 3.41, and 3.44 eV, respectively.

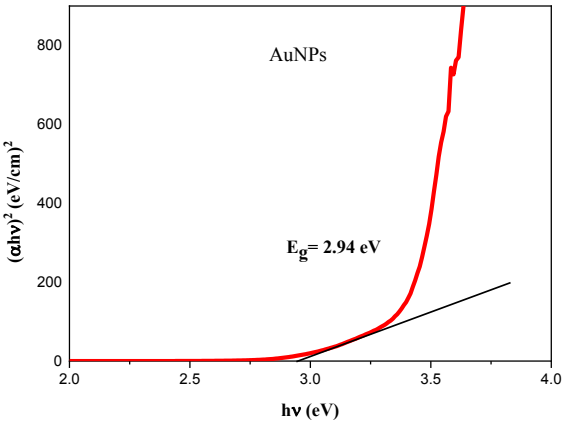

Fig. (6) The Tauc plot for Au nanoparticles

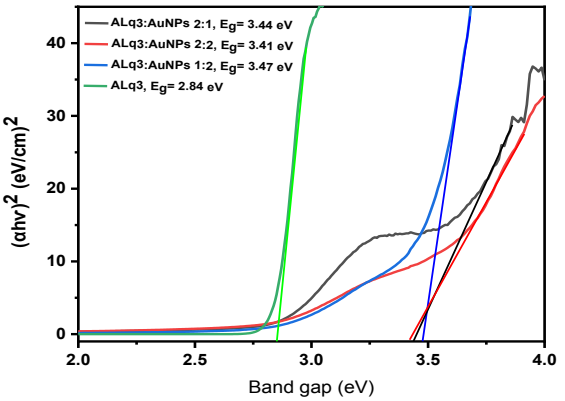

Fig. (7) Variation of $(\alpha h\upsilon)^2$ vs. photon energy for pure Alq_3 and Alq_3:AuNPs with different concentrations

The nonlinear optical properties of Au nanoparticles, pure Alq_3, and their nanocomposites at different mixing ratios were evaluated utilizing Z-scan experiment. As shown in Fig. (8), the closed-aperture Z-scan results exhibited a clear peak–valley pattern, which is a typical indicator of self-defocusing behavior. This confirms that all the studied samples have a negative nonlinear refractive index (n_2). The values of n_2 were estimated using Eq. (1) and found to be in the order of 10^{-11} m²/W, as presented in table (1).

Table (1) Nonlinear optical properties of prepared samples

Samples	α x10^3 (1/m)	$\Delta\emptyset_0$	n_2 x10^{-11} (m²/W)	ΔL_{p-v}
AuNPs	0.0455	3.181	1.26	1.2503
Alq_3:AuNPS 2:1	0.0872	6.005	2.86	2.36
Alq_3:AuNPs 2:2	0.0667	4.961	2.16	1.95
Alq_3:AuNPs 1:2	0.0624	5.699	2.4	2.24
Alq_3	0.222	9.083	7.2	3.57

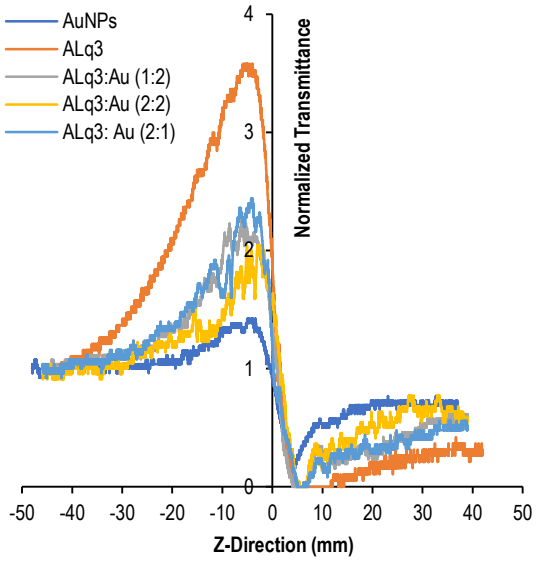

Fig. (8) Experimental results of the nonlinear transmittance through a closed aperture for AuNPs, pure Alq_3 and Alq_3:AuNPs with different concentrations

Pure Au nanoparticles showed a nonlinear refractive index of approximately 1.26×10^{-11} m²/W. A noticeable enhancement in the nonlinear optical response was observed when Au nanoparticles were incorporated into Alq_3, with the best performance recorded for the 2:1 Alq_3:AuNPs ratio. These findings suggest that such nanocomposites can be promising for use in nonlinear optical devices and optical shielding systems. Furthermore, the open-aperture Z-scan analysis, conducted under the same laser wavelength and low power, showed no evidence of nonlinear absorption in any of the tested materials, as indicated in table (1).

4. Conclusions

Gold nanoparticles were synthesized successfully via pulsed laser ablation and combined with Alq_3 at different volume ratios to prepare nanocomposite solutions. Structural analysis confirmed the formation of crystalline Au nanoparticles with nanoscale size. A distinct plasmonic peak was revealed at 340 nm for Au nanoparticles and a blue shift upon the addition of Alq_3 , indicating interaction between the components. A negative values of the nonlinear refractive index (n_2) were revealed, confirming self-defocusing behavior in all samples. The highest nonlinear response was observed in pure Alq_3 (7.2×10^{-11} m²/W), while the 2:1 Alq_3:AuNPs exhibited enhanced nonlinearity compared to Au nanoparticles alone. These findings demonstrate that incorporating Alq_3 improves the nonlinear optical response of gold nanoparticles and that Alq_3:AuNPs nanocomposites are promising for photonic and optical limiting applications.

Acknowledgement

The authors express their gratitude to the Department of Physics at the College of Science, University of Baghdad.

References

[1] H.N. Naser et al., "Green synthesis of novel chitosan-graphene oxide-silver nanoparticle nanocomposite for broad-spectrum antibacterial applications", *Oxford Open Mater. Sci.,* 5(1) (2025) itae018.

[2] K.D. Kim, D.N. Han and H.T. Kim, "Optimization of experimental conditions based on the Taguchi robust design for the formation of nano-sized silver particles by chemical reduction method", *Chem. Eng. J.,* 104(1–3) (2004) 55–61.

[3] L.A. Abdullah et al., "The influence of gold nanoparticles on electro-optical properties of nematic liquid crystal", *J. Opt.*, 53(2) (2024) 997–1002.

[4] M. Haruta, "Gold as a novel catalyst in the 21st century: Preparation, working mechanism and applications", *Gold Bull*., 37(1) (2004) 27–36.

[5] I.M. Ibrhim, "Synthesis and characteristics of Ag, Cu/Au Core/Shell nanoparticles produced by pulse laser ablation", *Iraqi J. Sci.,* 58(3C) (2017) 1651–1659.

[6] P. Zhao, N. Li and D. Astruc, "State of the art in gold nanoparticle synthesis", *Coord. Chem. Rev.*, 257(3–4) (2013) 638–665.

[7] A.H. Al-Hamdani, R. Amadlool and N.Z. Abdulazeez, "Effect of gold nanoparticle size on the linear and nonlinear optical properties", *AIP Conf. Proc.,* 2290 (2020) 4–11.

[8] M. Cuba and G. Muralidharan, "Effect of thermal annealing on the structural and optical properties of tris-(8-hydroxyquinoline) aluminum (III)(Alq_3) films", *Luminescence*, 30(3) (2015) 352–357.

[9] P. Dalasiński et al., "Study of optical properties of TRIS (8-hydroxyquinoline) aluminum (III)", *Opt. Mater.,* 28(1–2) (2006) 98–101.

[10] M.M. Duvenhage, O.M. Ntwaeaborwa and H.C. Swart, "Optical and chemical properties of Alq_3:PMMA blended thin films", *Mater. Today Proc.*, 2(7) (2015) 4019–4027.

[11] T. Cw, "Organic electroluminescent diodes", *Appl. Phys. Lett*., 51 (1987) 913–915.

[12] H.R. Mohammed and O.A. Ibrahim, "Electroluminescence of light-Emitting organic semiconductor/Europium oxide nanoparticle hybrid junction", *Iraqi J. Sci.,* 61(8) (2020) 1952–1959.

[13] H.H. Fong and S.K. So, "Hole transporting properties of tris (8-hydroxyquinoline) aluminum (Alq_3)", *J. Appl. Phys.*, 100(9) (2006) ??-??.

[14] A. Fuchs et al., "Molecular origin of differences in hole and electron mobility in amorphous Alq_3 - A multiscale simulation study", *Phys. Chem. Chem. Phys.,* 14(12) (2012) 4259–4270.

[15] L. Abdullah, "Nonlinear optical properties of liquid crystal doped with different concentrations of carbon nanotubes", *AIP Conf. Proc.,* ?? (2019) ??-??.

[16] M. Sheik-Bahae, A.A. Said and E.W. van Stryland, "High-sensitivity, single-beam n_2 measurements", *Opt. Lett.,* 14(17) (1989) 955–957.

[17] R.W. Boyd, **"Nonlinear Optics"**, 3rd ed., Academic Press (2008), Ch. 7.

[18] C. Suryanarayana et al., "Practical aspects of X-ray diffraction", *X-ray Diffr. A Pract. Approach*, 199863–199894.

[19] J. Tauc, "Optical properties and electronic structure of amorphous Ge and Si", *Mater. Res. Bull.,* 3(1) (1968) 37–46.

[20] A. Belahmar, A. Chouiyakh and M. Fahoume, "Structural and Optical Properties Evolution of Au/SiO_2 Nanocomposite Films", *The Influence of Substrate Temperature and Thermal Annealing, Open Access Libr. J.,* 4(9) (2017) 1–15.

